AGU PUBLICATIONS

Geophysical Research Letters

RESEARCH LETTER
10.1002/2017GL075831

Key Points:
- Two types of thousand-kilometer closed magnetic loops are identified in the Martian tail for the first time
- The occurrence rate of these closed loops is determined to range from a few tenths to a few tens percent
- These observations improve our understandings of Mars tail magnetic topology, cold ion escape, and reconnection

Supporting Information:
- Supporting Information S1

Correspondence to:
S. Xu,
shaosui.xu@ssl.berkeley.edu

Citation:
Shaosui, X., David, M., Janet, L., Yingjuan, M., Xiaohua F., Yuki, H., … DiBraccio, G. A. (2017). High-altitude closed magnetic loops at Mars observed by MAVEN. *Geophysical Research Letters*, *44*. https://doi.org/10.1002/2017GL075831

Received 29 SEP 2017
Accepted 28 OCT 2017
Accepted article online 2 NOV 2017

High-Altitude Closed Magnetic Loops at Mars Observed by MAVEN

Shaosui Xu[1], David Mitchell[1], Janet Luhmann[1], Yingjuan Ma[2], Xiaohua Fang[3], Yuki Harada[4], Takuya Hara[1], David Brain[3], Tristan Weber[3], Christian Mazelle[5], and Gina A. DiBraccio[6]

[1]Space Science Laboratory, University of California, Berkeley, CA, USA, [2]Department of Earth Planetary and Space Sciences, University of California, Los Angeles, CA, USA, [3]Laboratory of Atmospheric and Space Sciences, University of Colorado Boulder, Boulder, CA, USA, [4]Department of Physics and Astronomy, University of Iowa, Iowa City, IA, USA, [5]IRAP, University of Toulouse, CNRS, UPS, CNES, Toulouse, France, [6]NASA, Goddard Space Flight Center, Greenbelt, MD, USA

Abstract With electron and magnetic field data obtained by the Mars Atmosphere and Volatile EvolutioN (MAVEN) spacecraft, we have identified closed magnetic field lines, with both foot points embedded in the dayside ionosphere, extending up to 6,200 km altitude into the Martian tail. This topology is deduced from photoelectrons produced in the dayside ionosphere being observed traveling both parallel and antiparallel to the magnetic field. At trapped-zone pitch angles (within a range centered on 90° where electrons magnetically reflect before interacting with the atmosphere), cases with either solar wind electrons or photoelectrons have been found, indicating different formation mechanisms for these closed loops. These large closed loops are present in MHD simulations. The case with field-aligned photoelectrons mixed with solar wind electrons having trapped-zone pitch angles is likely to be associated with reconnection, while the case with photoelectrons at all pitch angles is probably due to closed field lines being pulled tailward by the surrounding plasma flow. By utilizing an algorithm for distinguishing photoelectrons from solar wind electrons in pitch angle-resolved energy spectra, we systematically map the spatial distribution and occurrence rate of these closed magnetic loops over the region sampled by the MAVEN orbit. We find that the occurrence rate ranges from a few percent to a few tens of percent outside of the optical shadow and less than one percent within the shadow. These observations can be used to investigate the general magnetic topology in the tail, which is relevant to cold ion escape, reconnection, and flux ropes.

1. Introduction

With intense localized crustal magnetic fields (e.g., Acuna et al., 1999; Connerney et al., 2005), Mars presents a complex obstacle to the solar wind, with both the ionosphere and crustal fields playing significant roles in the interaction. This is combined with an extended H and O corona, which begins to mass load the solar wind upstream of the bow shock. One result of this Mars-solar wind interaction is a complicated and dynamic magnetic topology (e.g., Brain et al., 2003, 2007; Liemohn, Ma, et al., 2006; Lillis & Brain, 2013; Ma et al., 2015; Steckiewicz et al., 2015; Xu, Mitchell, Liemohn, et al., 2016; Xu et al., 2017; Weber et al., 2017), which influences many aspects of the Mars plasma environment, such as reconnection (e.g., Halekas et al., 2006, 2009; Harada et al., 2015, 2017), the induced magnetosphere configuration (e.g., DiBraccio et al., 2015, 2017; Garnier et al., 2017; Liemohn et al., 2017; Luhmann et al., 2015; Xu, Liemohn, Dong, et al., 2016), planetary pickup ion transport (e.g., Fang et al., 2008), energetic electron precipitation (e.g., Fillingim et al., 2007; Lillis et al., 2009; Lillis & Brain, 2013; Shane et al., 2016; Xu et al., 2014), and auroral emission (e.g., Bertaux et al., 2005; Brain et al., 2006; Liemohn et al., 2007; Leblanc et al., 2008; Schneider et al., 2015; Shane et al., 2016).

Strong crustal fields rotate with the planet, therefore magnetic topology is expected to be complex and dynamic. This complexity has been investigated with numerical models (e.g., Brain et al., 2010; Brecht, 1997; Brecht & Ledvina, 2006; Bößwetter et al., 2007; Dong, Ma, et al., 2015; Fang et al., 2015; Harnett & Winglee, 2007; Kallio et al., 2006; Ledvina et al., 2008; Ma & Nagy, 2007; Modolo et al., 2016; Terada et al., 2009). Magnetic topology is one aspect of the system that is predicted by the models (e.g., Luhmann et al., 2015; Xu et al., 2017). MAVEN provides the opportunity to experimentally test and inform the models. This work

addresses one aspect of the topology, namely, closed magnetic loops that extend 2.8 Mars radii (R_m) into the tail (here defined as the region within the magnetic pileup boundary and downstream of the terminator plane). This particular picture of the topology is important because it tells us about both magnetosphere-like aspects of the Mars obstacle to the solar wind and the influence of reconnection processes, both of which can produce closed loops in the wake.

Above the superthermal electron exobase (~160 km, Xu, Liemohn, Bougher, et al., 2016), electrons with energies >1 eV experience few collisions with the neutral atmosphere and/or the thermal ionosphere and are thus constrained to gyrate about magnetic field lines on helical trajectories. Their fast motion (~1 R_m/s) and small gyroradii (less than a few kilometers) make them excellent tracers of magnetic topology. Brain et al. (2007) used pitch angle distributions to deduce the magnetic topology at 400 km with data from the Magnetometer/Electron Reflectometer (MAG/ER) instrument (Acuña et al., 1992; Mitchell et al., 2001) on board Mars Global Surveyor (MGS). The key of this method is that the presence of a loss cone indicates that the field line intersects the collisional atmosphere where the loss cone is formed. Another method to infer topology is to utilize the electron energy spectra to identify the plasma source regions sampled by the field line at large distances from the spacecraft. For example, the presence of ionospheric photoelectrons, identified by characteristic features at ~23 and ~60 eV, indicates that the field line intersects the dayside ionosphere (e.g., Frahm et al., 2006; Frahm et al., 2010; Liemohn, Frahm, et al., 2006; Liemohn, Ma, et al., 2006; Xu et al., 2014). This technique has also been used to determine magnetic connectivity to the dayside ionospheres of Venus and Titan (e.g., Coates et al., 2007, 2011; Wellbrock et al., 2012). However, as noted in Xu, Liemohn, Bougher, et al. (2016), it cannot be used to deduce the magnetic topology below source/loss altitudes, where collisions dominate electrons' motion, so we define a "foot point" as the location where a magnetic field line intersects the superthermal electron exobase (~160 km).

Previously, ionospheric photoelectrons observed at high altitudes in the tail were interpreted as an indicator of open field lines connected to the dayside ionosphere (e.g., Frahm et al., 2010; Liemohn, Ma, et al., 2006). In these studies, electron measurements could not be mapped into pitch angle because of the lack of simultaneous magnetic field measurements. Thus, there was no means of distinguishing a closed loop from an open field line embedded in the dayside ionosphere. While it was reasonable to associate these tail photoelectron observations with open field lines, since it is a more common configuration, it was not possible to explore other possible topologies.

Xu et al. (2017) was able to use pitch angle-resolved electron energy spectra from MAVEN to more accurately deduce the magnetic topology. Specifically, Xu et al. (2017) designed a shape parameter, a dimensionless number, that measures the deviation of a given electron energy spectrum from that of a canonical ionospheric photoelectron spectrum, which has discrete features at 23 and 27 eV due to ionization of CO_2 by the solar He II emission line at 30.4 nm, and at 60 eV due to a sharp drop in solar irradiance at wavelengths shorter than 17 nm (e.g., Frahm et al., 2006; Liemohn et al., 2003; Mitchell et al., 2000; Peterson et al., 2016). Small values indicate that the population is dominated by ionospheric photoelectrons; large values indicate that the population is of solar wind origin. Since both populations can be present simultaneously over a given pitch angle range, the shape parameter can have a continues range of values. Xu et al. (2017) found that a value less than unity allows us to confidently identify the presence of ionospheric photoelectrons, which means that the field line must sample the dayside ionosphere. This parameter can be calculated separately for parallel (source/loss cone pitch angles), antiparallel (also source/loss cone pitch angles), and perpendicular (trapped-zone pitch angles) populations. With simultaneous magnetic field measurements by the Magnetometer (MAG) (Connerney et al., 2015), parallel and antiparallel populations can be determined to have a velocity component pointing toward or away from Mars. Based on shape parameters of populations in each pitch angle range, Xu et al. (2017) mapped out the three-dimensional magnetic topology below 1,000 km. For example, a typical indication of a closed field line is the presence of photoelectrons (shape parameter <1) traveling both toward and away from the planet, which implies that both foot points are embedded in the ionosphere. In contrast, photoelectrons (shape parameter <1) traveling away from Mars and solar wind electrons (shape parameter >1) traveling toward Mars would indicate an open field line, as the field line has access to electron source regions in both the ionosphere and the solar wind.

With such a technique, we can determine the magnetic topologies associated with tail photoelectron observations, which is the topic of this study. The Mars Atmosphere and Volatile EvolutioN (MAVEN) spacecraft

(Jakosky, Lin, et al., 2015) carries a comprehensive set of particle and field instruments. With the data from the Solar Wind Electron Analyzer (SWEA) (Mitchell et al., 2016) and MAG, we here report observations that likely result from large closed loops with both foot points embedded in the dayside ionosphere as noted earlier. These observations help to improve our understanding of Mars' tail magnetic topology, cold ion escape (~1 eV), and reconnection.

2. Case Studies of High-Altitude Closed Loops

MAVEN is in a 75° inclination orbit with periapsis and apoapsis altitudes of ~150 and ~6,200 km. The orbit precesses in local time and latitude, so that during the first 2 years, the orbit swept across the tail five times over a range of altitudes. Two different categories of high-altitude closed magnetic field lines have been found in the tail, as defined by the electron populations observed over different pitch angle ranges: (1) photoelectrons in both parallel and antiparallel directions with a trapped population of solar wind electrons and (2) only photoelectrons in all directions. In this section, examples of these two types of observations will be examined.

2.1. Case 1: Mixed Electron Populations

Figure 1 shows a time series of spacecraft altitude (a), magnetic field magnitude (b) and components in the Mars Solar Orbital (MSO) frame (c) measured by MAG, pitch angle distributions (PAD) of 111 – 140 eV electrons (d), and electron energy spectra (e) measured by SWEA, and pitch angle-resolved shape parameters (f) on 14 February 2016. The MSO frame is centered on Mars, with X pointing toward the Sun, Y opposite to Mars' orbital angular velocity, and Z perpendicular to the orbital plane. Figure 1g shows the orbit geometry in MSO cylindrical frame. Figure 1h illustrates the SWEA observations for the first category: both field-aligned electron populations (blue and red spectra) are dominated by ionospheric photoelectrons, as indicated by the He II peak and the sharp decrease of electron fluxes near 60 eV. In contrast, the energy spectra for non-field-aligned electrons lack of these features, indicating that they are of solar wind origin. The shape parameters (Xu et al., 2017) for the directions toward and away from Mars are shown as the green and red lines in Figure 1f, respectively. The timing of the spectra in Figure 1h is indicated by the vertical dashed line. Note that the shape parameters for both field-aligned populations dip below 1 at this time, indicating the presence of ionospheric photoelectrons, consistent with the energy spectra.

The observation in Figure 1h, with ionospheric photoelectrons traveling both parallel (red) and antiparallel (blue) to the magnetic field, corresponding to shape parameters <1 in Figure 1f, indicates a closed field line with both foot points intersecting the dayside ionosphere. In this study, the dayside ionosphere refers to the sunlit hemisphere, instead of $X_{\mathrm{MSO}} > 0$. These two spectra (the blue and red spectra in Figure 1h) differ at low energies, implying that the two foot points of this field line embedded at different local times/solar zenith angles (e.g., Xu, Liemohn, Bougher, et al., 2015; Xu, Liemohn, Bougher, et al., 2016). This observation is made at 2,248 km altitude and $X_{\mathrm{MSO}} = -1.3\,R_m$. It suggests a large closed loop extending more than 1 R_m in size. The presence of solar wind electrons in the perpendicular pitch angles (the green spectrum in Figure 1h) suggests the field line was once open and had access to the solar wind. For this particular event, the spacecraft was observing closed field lines for roughly 1 min, which translates to ~180 km along the orbit track. According to the pitch angle distributions and energy spectra, the surrounding regions of these closed loops are populated by draped field lines, as no apparent loss cones or photoelectrons were observed. This information provides context for the formation of these closed loops.

2.2. Case 2: Photoelectrons Only

For case 2, we have chosen an orbit on 4 October 2015 (Figure 2). In Figure 2h, the photoelectron spectral features are seen in all three pitch angle ranges, and electron energy fluxes are about the same in each direction, indicating an isotropic distribution. Again, photoelectrons in both field-aligned directions indicate a closed field line with both foot points intersecting the dayside ionosphere. The trapped population is also photoelectrons, implying the field line has remained closed, with no access to solar wind, long enough for the perpendicular pitch angles to be populated with photoelectrons through pitch angle scattering. This observation is made at 2,550 km in altitude and $X_{\mathrm{MSO}} = -1.5R_m$, indicating a large closed loop extending downstream of the planet. In addition, in Figure 2e, a faint He II line can be seen from 17:30 UT to 18:40 UT, and in Figure 2f, the shape parameters for both directions are mostly below 1. Despite the uncertainty due to incomplete pitch angle coverage (Figure 2d), it is likely that the spacecraft is passing through a region of closed field lines from periapsis to 3,000 km in altitude.

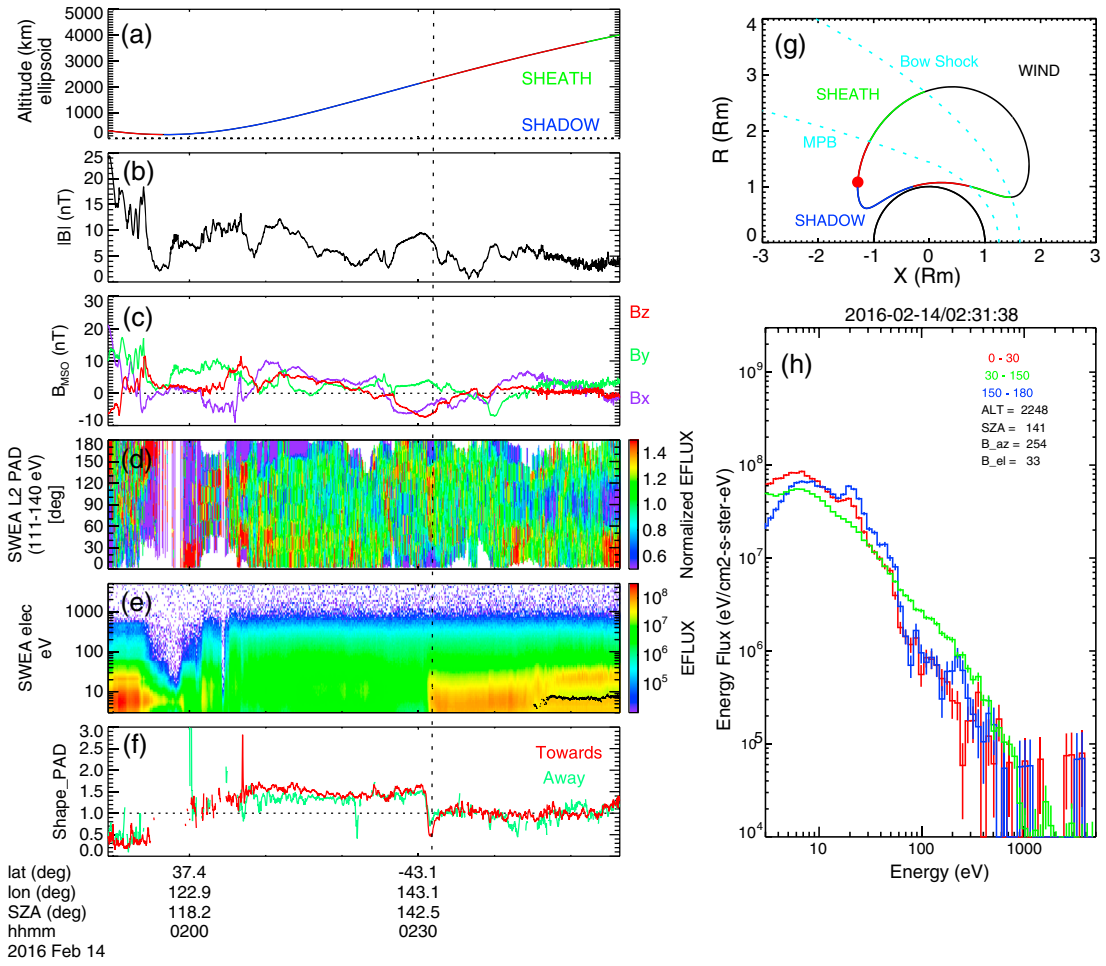

Figure 1. Time series of (a) spacecraft altitude, (b) magnetic field magnitude and (c) components in MSO coordinates measured by MAG, pitch angle distribution (PAD) of (d) 111–140 eV electrons, (e) energy spectra measured by SWEA, and (f) pitch angle-resolved shape parameters on 14 February 2016. The black dots in Figure 1e indicate the spacecraft potential estimated by SWEA measurements. In Figure 1f, "away" and "toward" indicate electron movement relative to the planet, determined from pitch angles and magnetic elevation angles. (g) The orbit geometry in MSO cylindrical frame, with *X* pointing at the Sun and R being the distance from the *X* axis. (h) The electron energy spectra for pitch angle (PA) 0°–30° (red), 30°–150° (green), and 150°–180° (blue), extracted at time indicated by the vertical dashed line in the left panels and the spacecraft location indicated by the red dot in Figure 1g. In Figures 1a and 1g, altitudes and orbit trajectories are colored according to nominal locations of the plasma regions, with fitted parameters from Trotignon et al. (2006). MPB refers to the magnetic pileup boundary.

3. Physical Interpretation

The Mars magnetic environment includes both "open" and "closed" field lines, whose identities change as the planet rotates (e.g., Fang et al., 2015; Ma et al., 2014) and/or solar wind conditions vary. Moreover, the closed fields can have both foot points on the day or night hemisphere, or one foot point on each. The case studies presented in Figures 1 and 2 show magnetic field lines extending >1.6 R_m into the tail with photoelectrons traveling in both the parallel and antiparallel directions. This indicates that both ends of the field line intersect the dayside ionosphere, which is the source of the photoelectrons. Such closed magnetic loops are present in MHD simulations. While MHD cannot describe all aspects of the Mars-solar wind interaction, and in particular the motion of energetic pickup ions, which can have gyroradii comparable to and larger than the size of the planet, previous studies (e.g., Dong, Fang, et al., 2015; Jakosky, Grebowsky, et al., 2015; Luhmann et al., 2015; Ma et al., 2015) have demonstrated that MHD simulations can resemble some aspects of the observed interaction. In this study, we use them as an interpretive tool, as magnetic topology is one area where MHD simulations could provide some insight. Conversely, we seek to inform such models with experimental measurements of Mars' topological configuration and its variability. Figure 3 displays a snapshot of closed and open field lines from the time-dependent MHD simulation of Ma et al. (2014) and Fang et al. (2015),

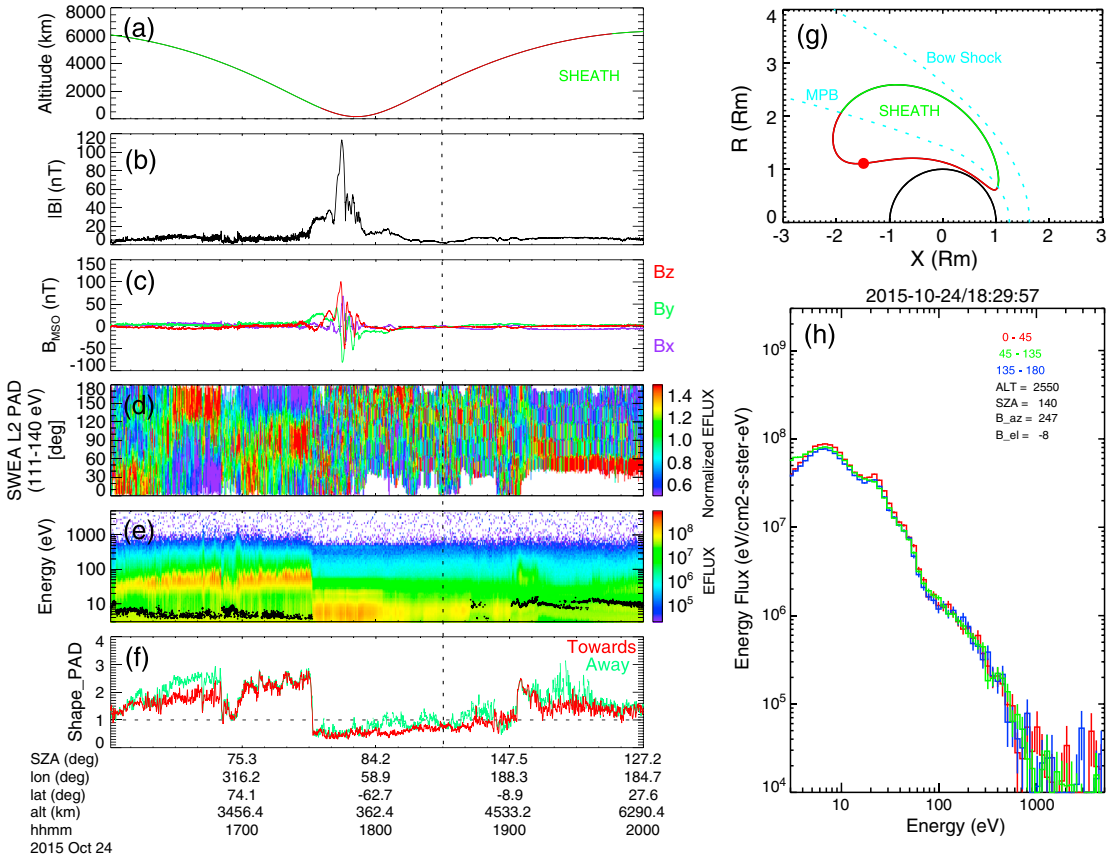

Figure 2. The ephemeris, magnetic field, and electron information of an orbit on 24 October 2015, the same format as Figure 1.

with magnetic field line tracing starting at 150 km. Several of the closed magnetic loops extending into the tail have both foot points in the dayside ionosphere (magenta lines on the $-Y_{MSO}$ side), which is the same configuration indicated by our experimental results.

The electron populations in the trapped-zone pitch angles differ for the two cases, implying different formation mechanisms and/or histories for the magnetic loops. For case 1, solar wind electrons are observed with pitch angles between 30° and 150° on a closed field line, indicating that they are trapped, or magnetically mirroring above the foot points. How do solar wind electrons become trapped on a closed magnetic field loop? Either solar wind electrons were injected onto the line at an earlier time when the magnetic topology was different or they drifted onto the field loop by magnetic gradient/curvature forces. Solar wind electrons have access to draped and open field lines in the tail; however, drift across these lines is unlikely because of the relatively large radii of field line curvature and small field gradients. These trapped solar wind electrons are more likely to result from the reconnection of two open field lines with a foot point embedded in the dayside ionosphere. While field-aligned solar wind electrons would be absorbed by the atmosphere within loss cone pitch angles (30° for Figure 1h) because of frequent collisions with atmospheric neutrals, solar wind electrons with more perpendicular pitch angles can survive and bounce above the collisional atmosphere until they pitch angle scatter into the loss cone. Meanwhile, field-aligned pitch angles will be continuously supplied with photoelectrons, as both foot points of the field line are embedded in the dayside ionosphere. In this scenario, our observations correspond to the state of the field line and electron populations after reconnection.

For case 2, the field line is populated with an isotropic distribution of photoelectrons, suggesting the field line has remained closed long enough for photoelectrons to scatter into the trapped zone. It is possible that case 2 is a more evolved stage of case 1: after sufficient time has passed for solar wind electrons to be scattered and lost to the atmosphere, and for photoelectrons to be scattered into the trapped zone of the pitch angle space. Another possible scenario is closed loops being distorted tailward by surrounding plasma flows.

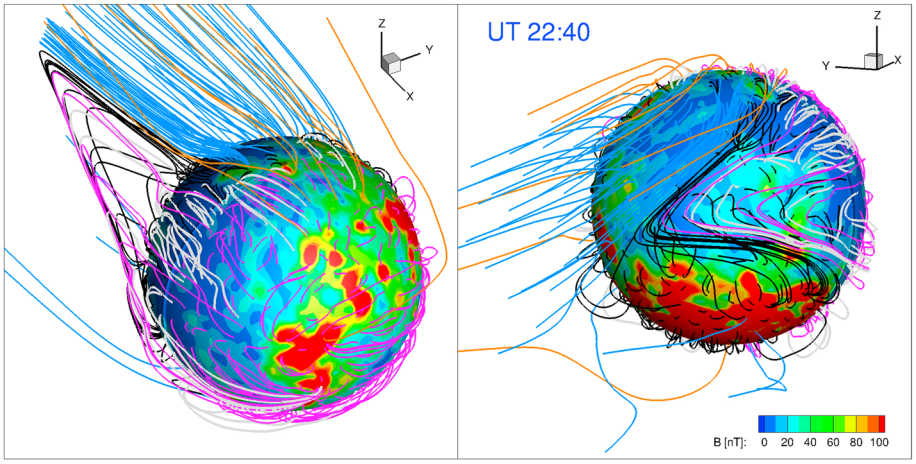

Figure 3. An example of magnetic field lines derived from a time-dependent MHD simulation by Ma et al. (2014) and Fang et al. (2015). The snapshot corresponds to a time point in the simulation when the strongest crustal field region is located on the nightside. The field lines have foot points at 150 km altitude on $10 \times 10°$ longitude-latitude grids. The color on the spherical surface is the magnetic magnitude at 105 km. As no draped solar wind-entriained field lines can penetrate down to such a low altitude, only closed and open field lines are shown, magenta for both foot points on the dayside, black for both foot points on the nightside, gray/white for cross terminator closed loops, orange for open field lines with one foot point on the dayside, and blue for open field lines with one foot point on the nightside.

In particular, the example in Figure 2, with a continuous transition from the ionosphere to closed loops extending to ~2,500 km altitude, suggests a large volume of closed field lines, supporting the second scenario. These large closed loops might be the prelude to high-altitude flux ropes (e.g., Hara et al., 2015).

4. Occurrence Rate

As the shape parameter is designed to distinguish photoelectrons from solar wind electrons, we can design an algorithm to search for closed magnetic loops with both foot points on the dayside ionosphere and with or without a trapped solar wind population throughout the MAVEN mission, from 1 December 2014 to 21 April 2017. Since the loss cone width is variable and not known a priori, the shape parameter is calculated for pitch angles (PAs) 0°–30°, 30°–150°, and 150°–180° separately. We choose a loss/source cone width of 30° to closely match the angular resolution of SWEA (22.5°). This provides near optimal sensitivity to the presence of photoelectrons while not excluding too much data because of insufficient pitch angle coverage. So for case 1, it requires the shape parameter below one for PA 0°–30° and 150°–180° and above one for PA 30°–150°; for case 2, the criterion is shape parameters below one for all three pitch angle ranges. On cross-terminator closed field lines (e.g., Collinson et al., 2016; Xu, Mitchell, Liemohn, et al., 2016), photoelectrons can be collisionally backscattered from the nightside atmosphere, but the reflected flux would be much lower. From a simulation with the Superthermal Electron Transport model (Liemohn et al., 2003; Xu & Liemohn, 2015; Xu, Liemohn, Peterson, et al., 2015), the reflected flux is around 10%–30% of incoming electron fluxes. Therefore, we only select samples with a flux ratio of the two field-aligned directions within a factor of 2 between 30 to 80 eV, to better ensure that both foot points are on the dayside.

The occurrence rates for case 1 and case 2 are illustrated in the left (a–c) and right (d–f) columns of Figure 4, respectively. The sample numbers for each projection are shown in Figure S1 in the supporting information. The occurrence rates range from a few percent to a few tens of percent outside of the optical shadow and <1% within the shadow and $X_{MSO} < -1.2$. The two cases share some similarities: a higher occurrence rate at low altitudes (the green and red areas in Figures 4c and 4f), as expected, and a higher occurrence rate outside of the shadow. The sharp change in occurrence rate at the wake boundary in all panels is likely not physical but rather is due to the negative spacecraft charging within the optical shadow. The spectra are corrected for spacecraft potential, but large values of the potential ($\lesssim -15$ V) increase the value of the shape parameter because part of the distribution is repelled by the potential. This results in an increased rate of misidentifications and an artificially lower occurrence rate of photoelectron spectra.

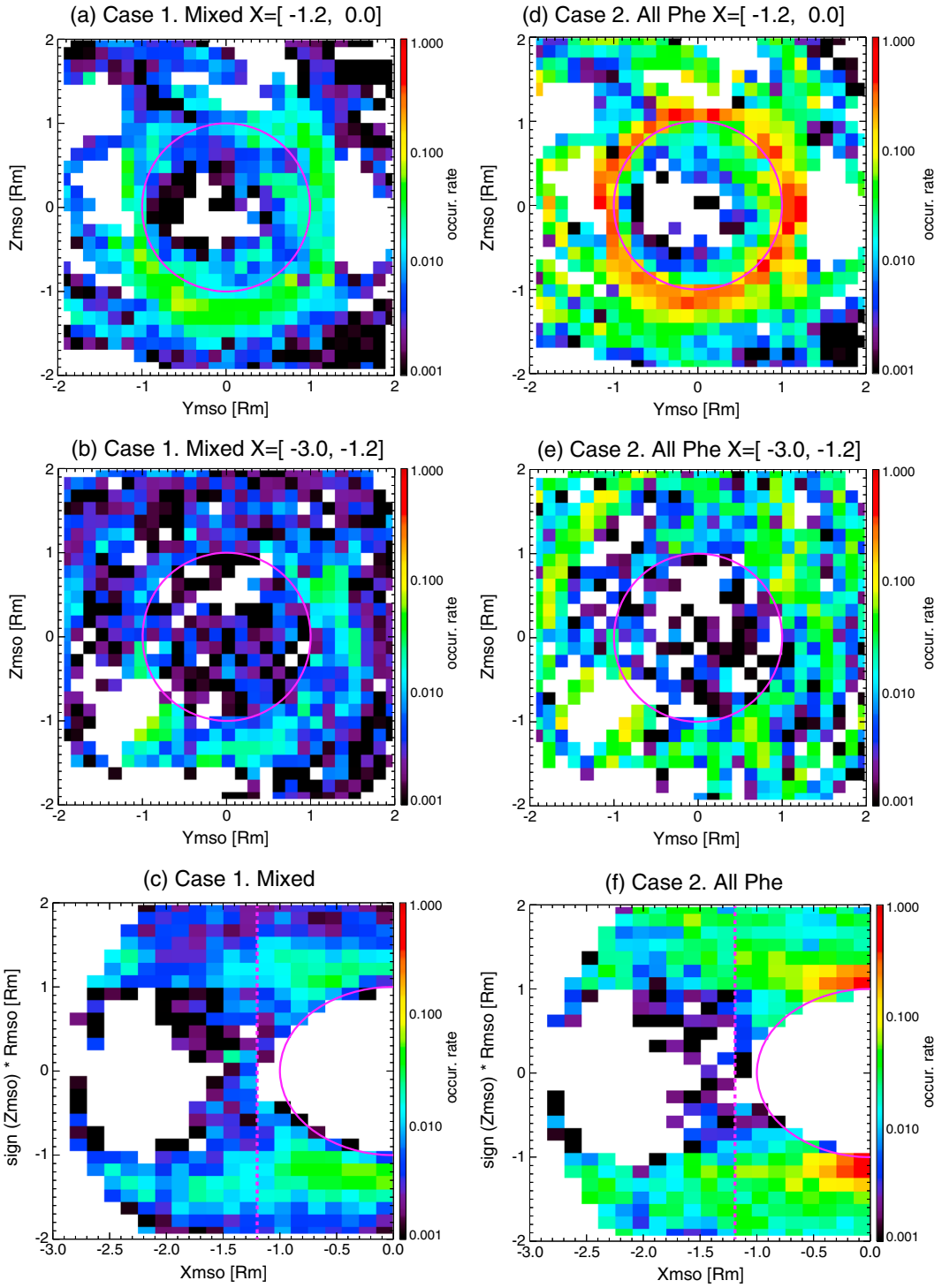

Figure 4. The occurrence rate of the high-altitude closed loops in three projections, the left column for case 1 and the right column for case 2. The top two rows are in the $Y_{MSO} - Z_{MSO}$ plane for two X_{MSO} ranges: (a–d) $X_{MSO} = [-1.2, 0]$ and (b and e) $X_{MSO} = [-3, -1.2]$, respectively, and (c and f) the MSO cylindrical coordinates with radial distance signed by $\pm Z_{MSO}$.

Outside the optical shadow, case 2 has higher occurrence rates than case 1, especially near the terminator plane (Figures 4c and 4f), where closed field lines are still in sunlight. Case 1 occurs more frequently in the $-Z_{MSO}$ hemisphere than the $+Z_{MSO}$ hemisphere from Figures 4a–4c, indirectly indicative of more reconnections in the southern hemisphere where the strongest crustal fields are located. Similarly, a higher occurrence rate in the $-Z_{MSO}$ hemisphere than the $+Z_{MSO}$ hemisphere is hinted in Figure 4f, arguably in Figures 4d and 4e, probably also attributed to the southern strong crustal fields.

Comparing Figures 4b and 4e, within the optical shadow, the occurrence rate of case 1 is higher than that of case 2. Other than the artifact caused by negative spacecraft potentials, there might be a physical explanation. Large loops are likely to be distorted into the tail because of the compression on the dayside and tailward plasma motion downstream. This stretching of closed loops is mostly in the antisunward direction, which makes it more difficult for such field lines to extend toward the X axis into the shadow.

5. Summaries and Implications

Using pitch angle-resolved electron energy spectra measured by SWEA, we have discovered closed magnetic loops, with both ends embedded in the dayside ionosphere, that extend up to at least 2.8 R_m downstream of the planet. While MHD has its limitations in describing Mars plasma environment, magnetic topology is one aspect where MHD models can provide insight. These large loops inferred from our observational study have appeared in MHD simulations driven by nominal solar wind parameters. It suggests that such large closed loops can routinely develop under quiet solar conditions. The two types of closed loops differ in formation mechanisms. For the case with a mixture of photoelectrons and solar wind electrons (case 1), it is likely a result of reconnection. The result is consistent with the spatial distributions of reconnection signature by Harada et al. (2017). For the case with photoelectrons in all directions (case 2), a possible scenario is that these closed field lines are pulled back down tail as crustal fields are compressed on the dayside and tailward plasma motion drags these field lines tail ward. The statistical results show that these large closed loops occur more frequently in the $-Z_{MSO}$ hemisphere, probably attributed to the southern strong crustal fields.

Previously, photoelectrons observed in the tail have been taken to be an indicator of open field lines connected to the dayside ionosphere and associated with tail ion escape (e.g., Coates et al., 2011; Frahm et al., 2010) due to instrumental limitations. These studies were conducted without a simultaneous magnetic field measurement, which could have been used to map the electron measurements into pitch angle and thus infer topology. This study suggests that tail photoelectron observations can also be indicative of closed field lines and, consequently, not necessarily lead to ion escape. Of course, we have shown that these loops experience reconnection, so what is trapped at one moment may be lost later. On the other hand, the low occurrence rate of these large closed loops suggests only a small correction to the presumed open magnetic topology in previous studies. As these large closed field lines are likely associated with reconnection, the occurrence map in Figure 4 is also suggestive of reconnection locations and occurrence rates, which are roughly consistent with findings in Harada et al. (2017). However, it is worth noticing that case 1 is only a subset of reconnection, excluding reconnections among closed, draped, and open field lines attached to the nightside. This is also part of reason why the occurrence rate within the shadow is much lower than that in Harada et al. (2017). In addition, these observations only serve as a snapshot of postreconnection. The reconnection site can be upstream or downstream of these observations. More likely it is the latter case if we assume recently closed loops move Marsward after reconnection. Electron transport simulations are needed to determine how long these trapped solar wind electrons can survive at high altitudes. Finally, Brain et al. (2010) illustrated a scenario, in which a large closed loop was pinched off and formed a flux rope. Case 2 could be a prelude of this scenario. The observations of high-altitude flux ropes by MAVEN (Hara et al., 2015) would be consistent with our study.

Acknowledgments
This work was supported by NASA grant NNH10CC04C to the University of Colorado and by subcontract to Space Sciences Laboratory, University of California, Berkeley. The MAVEN project is supported by NASA through the Mars Exploration Program.The MAVEN data used in this study are available through Planetary Data System (http://ppi.pds.nasa.gov/mission/MAVEN). The BATS-R-US code is publicly available from http://csem.engin.umich.edu/tools/swmf. The source data for Figure 3 are available at https://doi.org/10.6078/D1D37P.

References

Acuña, M., Connerney, J., Wasilewski, P., Lin, R., Anderson, K., Carlson, C., … Ness, N. F. (1992). Mars observer magnetic fields investigation. *Journal of Geophysical Research*, *97*(E5), 7799–7814.

Acuna, M., Connerney, J., Lin, R., Mitchell, D., Carlson, C., McFadden, J., … Cloutier, P. (1999). Global distribution of crustal magnetization discovered by the Mars Global Surveyor MAG/ER experiment. *Science*, *284*(5415), 790–793.

Bertaux, J.-L., Leblanc, F., Witasse, O., Quemerais, E., Lilensten, J., Stern, S., … Korablev, O. (2005). Discovery of an aurora on Mars. *Nature*, *435*(7043), 790–794.

Bößwetter, A., Simon, S., Bagdonat, T., Motschmann, U., Fränz, M., Roussos, E., … Lundin, R. (2007). Comparison of plasma data from ASPERA-3/Mars-Express with a 3-D hybrid simulation. *Annales Geophysicae*, *25*, 1851–1864. https://doi.org/10.5194/angeo-25-1851-2007

Brain, D., Bagenal, F., Acuña, M., & Connerney, J. (2003). Martian magnetic morphology: Contributions from the solar wind and crust. *Journal of Geophysical Research*, *108*, 1424. https://doi.org/10.1029/2002JA009482

Brain, D., Baker, A., Briggs, J., Eastwood, J., Halekas, J., & Phan, T.-D. (2010). Episodic detachment of Martian crustal magnetic fields leading to bulk atmospheric plasma escape. *Geophysical Research Letters*, *37*, L14108. https://doi.org/10.1029/2010GL043916

Brain, D., Barabash, S., Boesswetter, A., Bougher, S., Brecht, S., Chanteur, G., … Terada, N. (2010). A comparison of global models for the solar wind interaction with Mars. *Icarus*, *206*, 139–151. https://doi.org/10.1016/j.icarus.2009.06.030

Brain, D., Halekas, J., Peticolas, L., Lin, R., Luhmann, J., & Mitchell, D. (2006). On the origin of aurora on Mars. *Geophysical Research Letters*, *33*, L01201. https://doi.org/10.1029/2005GL024782

Brain, D., Lillis, R., Mitchell, D., Halekas, J., & Lin, R. (2007). Electron pitch angle distributions as indicators of magnetic field topology near Mars. *Journal of Geophysical Research*, *112*, A09201. https://doi.org/10.1029/2007JA012435

Brecht, S. H. (1997). Hybrid simulations of the magnetic topology of Mars. *Journal of Geophysical Research*, *102*, 4743–4750. https://doi.org/10.1029/96JA03205

Brecht, S. H., & Ledvina, S. A. (2006). The solar wind interaction with the Martian ionosphere/atmosphere. *Space Science Review*, *126*, 15–38. https://doi.org/10.1007/s11214-006-9084-z

Coates, A., Crary, F., Young, D., Szego, K., Arridge, C., Bebesi, Z., … Hill, T. (2007). Ionospheric electrons in Titan's tail: Plasma structure during the Cassini T9 encounter. *Geophysical Research Letters*, *34*, L24S05. https://doi.org/10.1029/2007GL030919

Coates, A. J., Tsang, S., Wellbrock, A., Frahm, R., Winningham, J., Barabash, S., … Crary, F. (2011). Ionospheric photoelectrons: Comparing Venus, Earth, Mars and Titan. *Planetary and Space Science*, *59*(10), 1019–1027.

Collinson, G., Mitchell, D., Xu, S., Glocer, A., Grebowsky, J., Hara, T., … Jakosky, B. (2016). Electric Mars: A large trans-terminator electric potential drop on closed magnetic field lines above Utopia Planitia. *Journal of Geophysical Research: Space Physics*, *122*, 2260–2271. https://doi.org/10.1002/2016JA023589

Connerney, J., Acuña, M., Ness, N., Kletetschka, G., Mitchell, D., Lin, R., & Reme, H. (2005). Tectonic implications of Mars crustal magnetism. *Proceedings of the National Academy of Sciences of the United States of America*, *102*(42), 14,970–14,975.

Connerney, J., Espley, J., Lawton, P., Murphy, S., Odom, J., Oliversen, R., & Sheppard, D. (2015). The MAVEN magnetic field investigation. *Space Science Reviews*, *195*(1–4), 257–291.

DiBraccio, G. A., Espley, J., Gruesbeck, J. R., Connerney, J. E., Brain, D. A., Halekas, J. S., … Jakosky, B. M. (2015). Magnetotail dynamics at Mars: Initial MAVEN observations. *Geophysical Research Letters*, *42*, 8828–8837. https://doi.org/10.1002/2015GL065248

DiBraccio, G. A., Dann, J., Espley, J. R., Gruesbeck, J. R., Soobiah, Y., Connerney, J. E. P., … Jakosky, B. M. (2017). Maven observations of tail current sheet flapping at mars. *Journal of Geophysical Research: Space Physics*, *122*, 4308–4324. https://doi.org/10.1002/2016JA023488

Dong, Y., Fang, X., Brain, D., McFadden, J., Halekas, J., Connerney, J., … Jakosky, B. (2015). Strong plume fluxes at Mars observed by MAVEN: An important planetary ion escape channel. *Geophysical Research Letters*, *42*, 8942–8950. https://doi.org/10.1002/2015GL065346

Dong, C., Ma, Y., Bougher, S. W., Toth, G., Nagy, A. F., Halekas, J. S., … Grebowsky, J. M. (2015). Multifluid MHD study of the solar wind interaction with Mars' upper atmosphere during the 2015 March 8th ICME event. *Geophysical Research Letters*, *42*, 9103–9112. https://doi.org/10.1002/2015GL065944

Fang, X., Liemohn, M. W., Nagy, A. F., Ma, Y., De Zeeuw, D. L., Kozyra, J. U., & Zurbuchen, T. H. (2008). Pickup oxygen ion velocity space and spatial distribution around Mars. *Journal of Geophysical Research*, *113*, A02210. https://doi.org/10.1029/2007JA012736

Fang, X., Ma, Y., Brain, D., Dong, Y., & Lillis, R. (2015). Control of Mars global atmospheric loss by the continuous rotation of the crustal magnetic field: A time-dependent mhd study. *Journal of Geophysical Research: Space Physics*, *120*, 10,926–10,944. https://doi.org/10.1002/2015JA021605

Fillingim, M. O., Peticolas, L. M., Lillis, R. J., Brain, D. A., Halekas, J. S., Mitchell, D. L., … Kirchner, D. L. (2007). Model calculations of electron precipitation induced ionization patches on the nightside of Mars. *Geophysical Research Letters*, *34*, L12101. https://doi.org/10.1029/2007GL029986

Frahm, R., Sharber, J., Winningham, J., Wurz, P., Liemohn, M., Kallio, E., … Mckenna-Lawler, S (2006). Locations of atmospheric photoelectron energy peaks within the Mars environment. *Space Science Reviews*, *126*(1–4), 389–402.

Frahm, R., Sharber, J., Winningham, J., Link, R., Liemohn, M., Kozyra, J., … Fedorov, A. (2010). Estimation of the escape of photoelectrons from Mars in 2004 liberated by the ionization of carbon dioxide and atomic oxygen. *Icarus*, *206*(1), 50–63.

Garnier, P., Steckiewicz, M., Mazelle, C., Xu, S., Mitchell, D., Holmberg, M. K. G., … Jakosky, B. M. (2017). The Martian photoelectron boundary as seen by MAVEN. *Journal of Geophysical Research: Space Physics*, *122*. https://doi.org/10.1002/2017JA024497

Halekas, J., Brain, D., Lillis, R., Fillingim, M., Mitchell, D., & Lin, R. (2006). Current sheets at low altitudes in the Martian magnetotail. *Geophysical Research Letters*, *33*, L13101. https://doi.org/10.1029/2006GL026229

Halekas, J., Eastwood, J., Brain, D., Phan, T., Øieroset, M., & Lin, R. (2009). In situ observations of reconnection hall magnetic fields at Mars: Evidence for ion diffusion region encounters. *Journal of Geophysical Research*, *114*, A11204. https://doi.org/10.1029/2009JA014544

Hara, T., Mitchell, D. L., McFadden, J. P., Seki, K., Brain, D. A., Halekas, J. S., … Jakosky, B. M. (2015). Estimation of the spatial structure of a detached magnetic flux rope at Mars based on simultaneous maven plasma and magnetic field observations. *Geophysical Research Letters*, *42*, 8933–8941. https://doi.org/10.1002/2015GL065720

Harada, Y., Halekas, J., McFadden, J., Mitchell, D., Mazelle, C., & Connerney, J. (2015). Magnetic reconnection in the near-Mars magnetotail: MAVEN observations. *Geophysical Research Letters*, *42*, 8838–8845. https://doi.org/10.1002/2015GL065004

Harada, Y., Halekas, J. S., McFadden, J. P., Espley, J., DiBraccio, G. A., Mitchell, D. L., … Jakosky, B. M. (2017). Survey of magnetic reconnection signatures in the Martian magnetotail with MAVEN. *Journal of Geophysical Research: Space Physics*, *122*, 5114–5131. https://doi.org/10.1002/2017JA023952

Harnett, E. M., & Winglee, R. M. (2007). High-resolution multifluid simulations of the plasma environment near the Martian magnetic anomalies. *Journal of Geophysical Research*, *112*, A05207. https://doi.org/10.1029/2006JA012001

Jakosky, B. M., Grebowsky, J. M., Luhmann, J. G., Connerney, J., Eparvier, F., & Ergun, R. (2015). MAVEN observations of the response of Mars to an interplanetary coronal mass ejection. *Science*, *350*(6261), AAD0210.

Jakosky, B. M., Lin, R., Grebowsky, J., Luhmann, J., Mitchell, D., Beutelschies, G., … Zurek, R. (2015). The Mars Atmosphere and Volatile Evolution (MAVEN) mission. *Space Science Reviews*, *195*(1–4), 3–48.

Kallio, E., Fedorov, A., Budnik, E., Säles, T., Janhunen, P., Schmidt, W., … Dierker, C. (2006). Ion escape at Mars: Comparison of a 3-D hybrid simulation with Mars Express IMA/ASPERA-3 measurements. *Icarus*, *182*, 350–359. https://doi.org/10.1016/j.icarus.2005.09.018

Leblanc, F., Witasse, O., Lilensten, J., Frahm, R. A., Safaenili, A., Brain, D. A., … Lundin, R. (2008). Observations of aurorae by SPICAM ultraviolet spectrograph on board Mars Express: Simultaneous ASPERA-3 and MARSIS measurements. *Journal of Geophysical Research*, *113*, A08311. https://doi.org/10.1029/2008JA013033

Liemohn, M. W., Frahm, R. A., Winningham, J. D., Ma, Y., Barabash, S., Lundin, R., … Dierker, C. (2006). Numerical interpretation of high-altitude photoelectron observations. *Icarus*, *182*, 383–395. https://doi.org/10.1016/j.icarus.2005.10.036

Liemohn, M. W., Ma, Y., Frahm, R. A., Fang, X., Kozyra, J. U., Nagy, A. F., … Lundin, R. (2006). Mars global MHD predictions of magnetic connectivity between the dayside ionosphere and the magnetospheric flanks. *Space Science Reviews*, *126*, 63–76. https://doi.org/10.1007/s11214-006-9116-8

Ledvina, S. A., Ma, Y.-J., & Kallio, E. (2008). Modeling and simulating flowing plasmas and related phenomena. *Space Science Review*, *139*, 143–189. https://doi.org/10.1007/s11214-008-9384-6

Liemohn, M. W., Ma, Y., Nagy, A., Kozyra, J., Winningham, J., Frahm, R., … Lundin, R. (2007). Numerical modeling of the magnetic topology near Mars auroral observations. *Geophysical Research Letters*, *34*, L24202. https://doi.org/10.1029/2007GL031806

Liemohn, M. W., Mitchell, D. L., Nagy, A. F., Fox, J. L., Reimer, T. W., & Ma, Y. (2003). Comparisons of electron fluxes measured in the crustal fields at Mars by the mgs magnetometer/electron reflectometer instrument with a B field-dependent transport code. *Journal of Geophysical Research*, *108*(E12), 5134. https://doi.org/10.1029/2003JE002158

Liemohn, M. W., Xu, S., Dong, C., Bougher, S. W., Johnson, B. C., Ilie, R., & De Zeeuw, D. L. (2017). Ionospheric control of the dawn-dusk asymmetry of the Mars magnetotail current sheet. *Journal of Geophysical Research: Space Physics*, *122*, 6397–6414. https://doi.org/10.1002/2016JA023707

Lillis, R. J., & Brain, D. A. (2013). Nightside electron precipitation at Mars: Geographic variability and dependence on solar wind conditions. *Journal of Geophysical Research: Space Physics*, *118*, 3546–3556. https://doi.org/10.1002/jgra.50171

Lillis, R. J., Fillingim, M. O., Peticolas, L. M., Brain, D. A., Lin, R. P., & Bougher, S. W. (2009). Nightside ionosphere of Mars: Modeling the effects of crustal magnetic fields and electron pitch angle distributions on electron impact ionization. *Journal of Geophysical Research*, *114*, E11009. https://doi.org/10.1029/2009JE003379

Luhmann, J., Dong, C., Ma, Y., Curry, S., Mitchell, D., & Espley, J. (2015). Implications of MAVEN Mars near-wake measurements and models. *Geophysical Research Letters*, *42*, 9087–9094. https://doi.org/10.1002/2015GL066122

Ma, Y., Fang, X., Russell, C. T., Nagy, A. F., Toth, G., Luhmann, J. G., … Dong, C. (2014). Effects of crustal field rotation on the solar wind plasma interaction with Mars. *Geophysical Research Letters*, *41*, 6563–6569. https://doi.org/10.1002/2014GL060785

Ma, Y., Russell, C., Fang, X., Dong, Y., Nagy, A., Toth, G., … Jakosky, B. M. (2015). MHD model results of solar wind interaction with Mars and comparison with MAVEN plasma observations. *Geophysical Research Letters*, *42*, 9113–9120. https://doi.org/10.1002/2015GL065218

Ma, Y.-J., & Nagy, A. F. (2007). Ion escape fluxes from Mars. *Geophysical Research Letters*, *34*, L08201. https://doi.org/10.1029/2006GL029208

Mitchell, D., Lin, R., Reme, H., Crider, D., Cloutier, P., Connerney, J., … Ness, N. (2000). Oxygen auger electrons observed in Mars' ionosphere. *Geophysical research letters*, *27*(13), 1871–1874.

Mitchell, D., Lin, R., Mazelle, C., Reme, H., Cloutier, P., Connerney, J., … Ness, N. (2001). Probing Mars' crustal magnetic field and ionosphere with the MGS electron reflectometer. *Journal of Geophysical Research*, *106*(E10), 23,419–23,427.

Mitchell, D., Mazelle, C., Sauvaud, J.-A., Thocaven, J.-J., Rouzaud, J., Fedorov, A., … Jakosky, B. M. (2016). The MAVEN solar wind electron analyzer. *Space Science Reviews*, *200*(1–4), 495–528.

Modolo, R., Hess, S., Mancini, M., Leblanc, F., Chaufray, J.-Y., Brain, D., … Mazelle, C. (2016). Mars-solar wind interaction: Lathys, an improved parallel 3-D multispecies hybrid model. *Journal of Geophysical Research: Space Physics*, *121*, 6378–6399. https://doi.org/10.1002/2015JA022324

Peterson, W., Thiemann, E., Eparvier, F. G., Andersson, L., Fowler, C., Larson, D., … Jakosky, B. (2016). Photoelectrons and solar ionizing radiation at Mars: Predictions versus maven observations. *Journal of Geophysical Research: Space Physics*, *121*, 8859–8870. https://doi.org/10.1002/2016JA022677

Schneider, N. M., Deighan, J. I., Jain, S. K., Stiepen, A., Stewart, A. I. F., & Larson, D. (2015). Discovery of diffuse aurora on Mars. *Science*, *350*(6261), AAD0313.

Shane, A. D., Xu, S., Liemohn, M. W., & Mitchell, D. L. (2016). Mars nightside electrons over strong crustal fields. *Journal of Geophysical Research: Space Physics*, *121*, 3808–3823. https://doi.org/10.1002/2015JA021947

Steckiewicz, M., Mazelle, C., Garnier, P., André, N., Penou, E., Beth, A., … Jakosky, B. M. (2015). Altitude dependence of nightside Martian suprathermal electron depletions as revealed by MAVEN observations. *Geophysical Research Letters*, *42*, 8877–8884. https://doi.org/10.1002/2015GL065257

Terada, N., Kulikov, Y. N., Lammer, H., Lichtenegger, H. I. M., Tanaka, T., Shinagawa, H., & Zhang, T. (2009). Atmosphere and water loss from early Mars under extreme solar wind and extreme ultraviolet conditions. *Astrobiology*, *9*, 55–70. https://doi.org/10.1089/ast.2008.0250

Trotignon, J., Mazelle, C., Bertucci, C., & Acuña, M. (2006). Martian shock and magnetic pile-up boundary positions and shapes determined from the Phobos 2 and Mars global surveyor data sets. *Planetary and Space Science*, *54*(4), 357–369. https://doi.org/https://doi.org/10.1016/j.pss.2006.01.003

Weber, T., Brain, D., Mitchell, D., Xu, S., Connerney, J., & Halekas, J. (2017). Characterization of low altitude nightside Martian magnetic topology using electron pitch angle distributions. *Journal of Geophysical Research: Space Physics*, *122*. https://doi.org/10.1002/2017JA024491

Wellbrock, A., Coates, A. J., Sillanpää, I., Jones, G. H., Arridge, C. S., Lewis, G. R., … Aylward, A. D. (2012). Cassini observations of ionospheric photoelectrons at large distances from Titan: Implications for Titan's exospheric environment and magnetic tail. *Journal of Geophysical Research*, *117*, A03216. https://doi.org/10.1029/2011JA017113

Xu, S., & Liemohn, M. W. (2015). Superthermal electron transport model for Mars. *Earth and Space Science*, *2*(3), 47–64. https://doi.org/10.1002/2014EA000043

Xu, S., Liemohn, M., Bougher, S., & Mitchell, D. (2015). Enhanced carbon dioxide causing the dust storm-related increase in high-altitude photoelectron fluxes at Mars. *Geophysical Research Letters*, *42*(22), 9702–9710.

Xu, S., Liemohn, M., Bougher, S., & Mitchell, D. (2016). Martian high-altitude photoelectrons independent of solar zenith angle. *Journal of Geophysical Research: Space Physics*, *121*, 3767–3780. https://doi.org/10.1002/2015JA022149

Xu, S., Liemohn, M. W., Dong, C., Mitchell, D. L., Bougher, S. W., & Ma, Y. (2016). Pressure and ion composition boundaries at mars. *Journal of Geophysical Research: Space Physics*, *121*, 6417–6429. https://doi.org/10.1002/2016JA022644

Xu, S., Liemohn, M. W., & Mitchell, D. L. (2014). Solar wind electron precipitation into the dayside Martian upper atmosphere through the cusps of strong crustal fields. *Journal of Geophysical Research: Space Physics*, *119*, 10,100–10,115. https://doi.org/10.1002/2014JA020363

Xu, S., Liemohn, M. W., Peterson, W., Fontenla, J., & Chamberlin, P. (2015). Comparison of different solar irradiance models for the superthermal electron transport model for mars. *Planetary and Space Science*, *119*, 62–68.

Xu, S., Mitchell, D., Liemohn, M., Dong, C., Bougher, S., Fillingim, M., … Jakosky, B. (2016). Deep nightside photoelectron observations by MAVEN SWEA: Implications for Martian northern hemispheric magnetic topology and nightside ionosphere source. *Geophysical Research Letters*, *43*, 8876–8884. https://doi.org/10.1002/2016GL070527

Xu, S., Mitchell, D., Liemohn, M., Fang, X., Ma, Y., Luhmann, J., … Jakosky, B. (2017). Martian low-altitude magnetic topology deduced from MAVEN/SWEA observations. *Journal of Geophysical Research: Space Physics*, *122*, 1831–1852. https://doi.org/10.1002/2016JA023467